Behavior of the Blade Tip Vortices of a Wind Turbine Equipped with a Brimmed-Diffuser Shroud

Takahashi, Shuhei
Department of Aeronautics and Astronautics, Kyushu University

Hata, Yuya
Department of Aeronautics and Astronautics, Kyushu University

Ohya, Yuji
Research Institute for Applied Mechanics, Kyushu University

Karasudani, Takashi
Research Institute for Applied Mechanics, Kyushu University

他

出版情報：Energies. 5 (12), pp.5229-5242, 2012-12. MDPI
バージョン：

Energies **2012**, *5*, 5229-5242; doi:10.3390/en5125229

OPEN ACCESS

energies

ISSN 1996-1073

www.mdpi.com/journal/energies

Article

Behavior of the Blade Tip Vortices of a Wind Turbine Equipped with a Brimmed-Diffuser Shroud

Shuhei Takahashi [1,*], Yuya Hata [1], Yuji Ohya [2], Takashi Karasudani [2] and Takanori Uchida [2]

[1] Department of Aeronautics and Astronautics, Kyushu University, Kasuga, Fukuoka 816-8580, Japan; E-Mail: k-watana@riam.kyushu-u.ac.jp

[2] Research Institute for Applied Mechanics, Kyushu University, Kasuga, Fukuoka 816-8580, Japan; E-Mails: ohya@riam.kyushu-u.ac.jp (Y.O.); karasu@riam.kyushu-u.ac.jp (T.K.); takanori@riam.kyushu-u.ac.jp (T.U.)

* Author to whom correspondence should be addressed; E-Mail: swvawt@hotmail.co.jp; Tel.: +81-92-583-7777; Fax: +81-92-583-7779.

Received: 3 November 2012; in revised form: 30 November 2012 / Accepted: 10 December 2012 / Published: 13 December 2012

Abstract: To clarify the behavior of the blade tip vortices of a wind turbine equipped with a brimmed-diffuser shroud, called a "Wind-Lens turbine", we conducted a three-dimensional numerical simulation using a large eddy simulation (LES). Since this unique wind turbine consists of not only rotating blades but also a diffuser shroud with a broad-ring brim at the exit periphery, the flow field around the turbine is highly complex and unsteady. Previously, our research group conducted numerical simulations using an actuator-disc approximation, in which the rotating blades were simply modeled as an external force on the fluid. Therefore, the detailed flow patterns around the rotating blades and the shroud, including the blade tip vortices, could not be simulated. Instead of an actuator-disc approximation, we used a moving boundary technique in the present CFD simulation to simulate the flow around a rotating blade in order to focus especially on blade tip vortices. The simulation results showed a pair of vortices consisting of a blade tip vortex and a counter-rotating vortex which was generated between the blade tip and the inner surface of the diffuser. Since these vortices interacted with each other, the blade tip vortex was weakened by the counter-rotating vortex. The results showed good agreement with past wind tunnel experiments.

Keywords: wind turbine; diffuser; brim; vortex; noise; numerical simulation

---

1. Introduction

To help solve energy problems and mitigate global warming, the importance of clean, renewable energy is growing. In addition, in order to prevent massive blackouts caused by disasters, small distributed energy systems have been and continue to be tested. In this testing, there has been an increase in the variety of technologies used to generate clean, renewable energy.

Of the clean, renewable energy generation methods, wind power generation, which can be conducted over the ocean, is attracting increasing attention. However, wind power generation has the following disadvantages: low output compared to thermal and nuclear power generation, noise, bird strikes, and landscape disturbances. Gilbert and Foreman [1] examined a diffuser-augmented wind turbine (DAWT) as a part of their research on high-power wind turbines. A DAWT is a wind turbine in which the power is augmented by concentrating the wind energy using a diffuser. We have developed a unique wind turbine with a brimmed diffuser called a "Wind-Lens turbine" [2,3]. An example of this turbine is shown in Figure 1. A Wind-Lens turbine consists of a downwind type wind turbine and a structure composed of an inlet shroud, a diffuser, and a brim. The flow which passes inside the diffuser and the flow which comes around behind the brim generate a large vortex behind the structure, as shown in Figure 2. As a result of this very low-pressure region, air is drawn into the turbine at a higher rate and accelerates more than in the case with a bare wind turbine. Due to this effect, a 3 kW turbine with a rotor diameter of 2.5 m generates 2.5 times more power with a Wind-Lens than the same turbine without a Wind-Lens.

Figure 1. Wind-Lens turbine (rated power of 3 kW at 11 m/s wind speed).

Figure 2. Characteristics of flow around a Wind-Lens turbine.

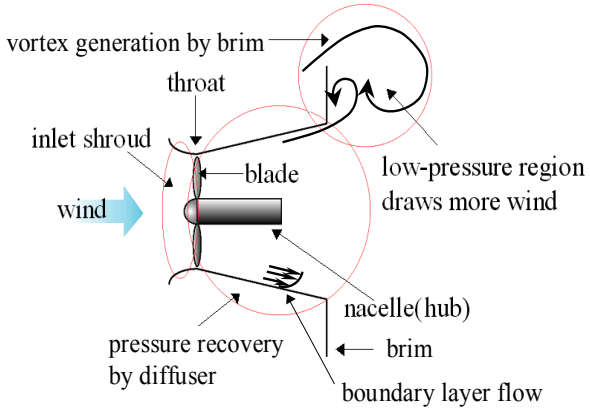

In addition to increased power output, a Wind-Lens turbine offers the following advantages: low noise, reduced number of bird strikes, and reduced landscape disturbance. Our research group's previous studies reported the power increase of Wind-Lens turbines [2,3]. In this paper, we focus on the low aerodynamic noise of Wind-Lens turbines. Figure 3 shows an example of a noise survey based on an international standard for measuring noise generated by wind turbines, JIS C1400-11 (IEC 61400-11). There is no appreciable difference in the noise level between a Wind-Lens turbine in operation and one at rest [4]. There are many sources of wind turbine noise including (1) turbulent boundary layer trailing edge noise; (2) laminar boundary layer vortex shedding noise; (3) boundary layer separation noise; and (4) noise associated with blade tip vortex formation [5]. In particular, blade tip vortices can strongly contribute to wind turbine noise over a broad band of high frequencies [6,7]. In this paper, we focus on blade tip vortices in a Wind-Lens turbine since the blades of a Wind-Lens turbine are enclosed by the Wind-Lens structure and thus the circumstance of the blade tips in a Wind-Lens turbine is quite different from that of the blade tips on a bare wind turbine. Therefore, we conducted numerical simulations of the flow around a Wind-Lens turbine, paying special attention to the behavior of the blade tip vortices.

Figure 3. An example of a noise survey for a Wind-Lens turbine [4].

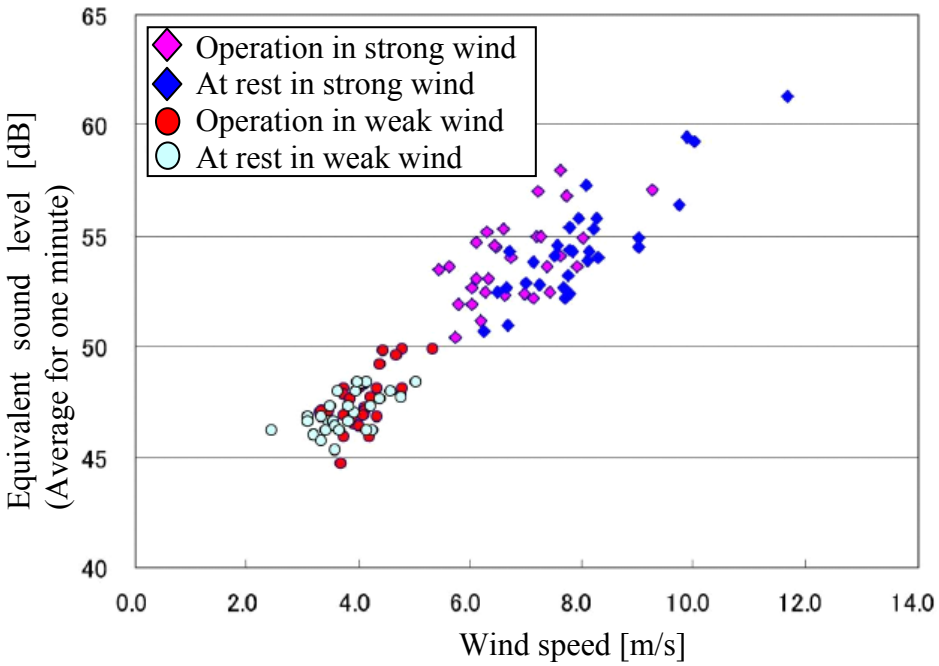

Numerical simulations of the flow around a Wind-Lens turbine have been conducted previously, however, almost all of these simulations used the Reynolds-averaged Navier-Stokes (RANS) technique. This numerical technique modeled a wind turbine as a simple resistance in the inflow direction [8,9]. For an unsteady 3D direct numerical simulation, an actuator-disk model for a wind turbine was devised to simulate the drag and rotational forces exerted on the fluid by the wind turbine [10]. A revised version of the actuator-disk model, an actuator-line model, represented the blades as rotating lines [11]. However, these models cannot simulate the details of the flow around a wind turbine such as the flow around a whole blade under rotation, the flow separation at the blade trailing edge, and the blade tip

vortices. Therefore, in the present paper, we use a moving boundary technique in the CFD model to simulate the flow around the rotating blades.

2. Numerical Simulation Method

Numerical simulations are conducted with the commercial CFD software STAR-CCM+, in which a finite-volume method and LES are used to solve the Navier–Stokes equations. The WALE model [12] is used as the subgrid-scale model in the LES. As mentioned above, we use a moving boundary technique in the present study. In this technique, the simulation region is divided into a static region and a rotating region. Data on the fluid flow, such as velocity and pressure data, are transferred between the static and rotating regions through the interface between them at every time step. A first-order implicit method is used for the time marching method. A second-order upwind scheme is applied to the convective term. Table 1 shows the simulation conditions.

The Reynolds number is defined as $\mathrm{Re} = DU_\infty/\nu$, where D is the diameter of the wind turbine rotor, U_∞ is the uniform inflow speed, and ν is the dynamic viscosity. The blade tip speed ratio is defined as $\lambda = \omega R/U_\infty$, where ω is the angular frequency of rotation of the blades and R is the radius of the wind turbine rotor. As for the boundary conditions, velocity is constant at the inflow boundary, pressure is constant at the outflow boundary, free-slip conditions are imposed at the far-field boundaries, and no-slip conditions are imposed on the surface of objects.

Since there are three blades in a symmetrical configuration, we simulate one third of the rotor area and assume the periodicity condition on the boundaries indicated by blue dots in Figure 4. It should be noted that the numbers of cells in Table 1 are not enough to simulate the whole fields with high accuracy and more cells should be required. To simulate the behavior of the blade tip vortices, however, we concentrated the cells around the area between the blade tip and the inside wall and in the near downstream, as seen in Figure 5. Therefore the numerical simulation results in the present research show a good qualitative agreement with past wind tunnel experiments.

Figure 4. Simulation region of the long-type Wind-Lens turbine. *x*: inflow direction; *r*: radial direction; θ: circumferential direction.

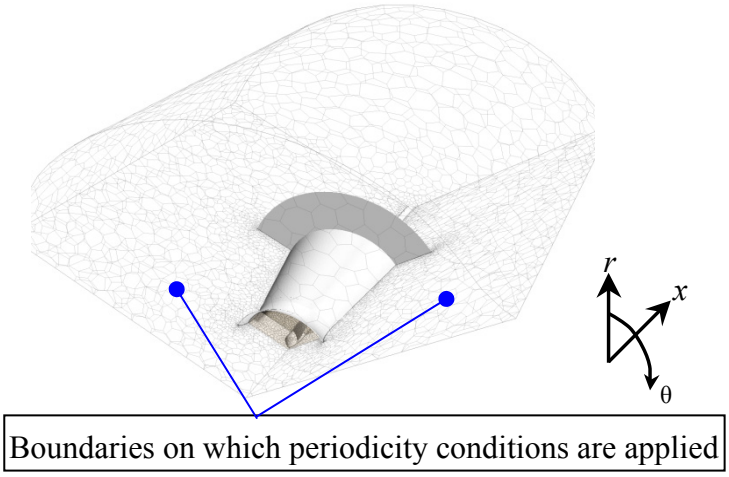

Figure 5. Calculation mesh for the long-type Wind-Lens turbine in an *x*-*r* cross-section. *x*: inflow direction; *r*: radial direction.

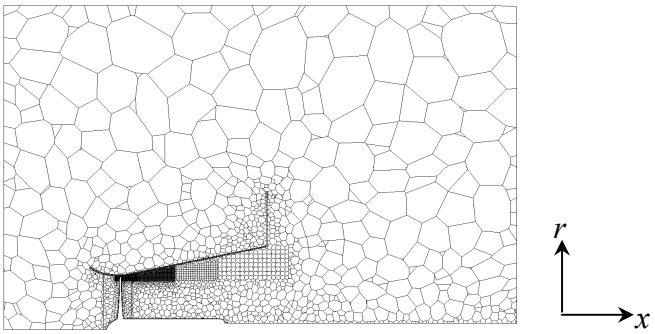

Table 1. Simulation conditions.

Type of wind turbine (see Figure 6)	Long-type wind-Lens turbine	Compact-type Wind-Lens turbine		Bare wind turbine
		For simulation of the blade tip vortices	For comparison with the bare wind turbine	
Reynolds number	1.65×10^5	7.98×10^5		7.98×10^5
Blade tip speed ratio	4.5	4.0		4.0
Time step	3×10^{-5}	3×10^{-4}	1×10^{-3}	1×10^{-3}
Number of cells	1,983,513	1,918,566	759,310	551,829

Figure 6 shows the objects considered in the simulations: (a) a long-type Wind-Lens turbine, which incorporates an elongated diffuser; (b) a compact-type Wind-Lens turbine; and (c) a bare wind turbine. Figure 7 and Table 2 show the configuration parameters of the Wind-Lens turbines. The configuration of the bare wind turbine is the same as that of the compact-type Wind-Lens turbine without the brimmed-diffuser shroud. As shown in Table 1, there are two calculation conditions for the compact-type Wind-Lens turbine: one condition is adopted to focus on the blade tip vortices and the other condition is adopted to focus on the differences between a bare wind turbine and a compact-type Wind-Lens turbine. Examples of the simulation region and mesh are shown in Figures 4 and 5. In these figures, the simulation region and mesh are shown for the long-type Wind-Lens turbine.

Table 2. Parameters for the configurations of the Wind-Lens turbines.

Type of Wind-Lens	Long-type	Compact-type
Type of blade	NACA	MEL
Diameter of the throat (D_t)	400 mm	2560 mm
Diameter of the rotor (D)	380 mm	2500 mm
Diameter of the hub (D_h)	88 mm	360 mm
Diffuser length (L)	500 mm	351 mm
Inlet length + Diffuser length (L_t)	600 mm	576 mm
Height of the brim (h)	200 mm	256 mm
Tip clearance (s)	10 mm	30 mm
Semi-open angle (θ)	12°	-

Figure 6. Objects considered in the simulations: (**a**) long-type Wind-Lens turbine; (**b**) compact-type Wind-Lens turbine; (**c**) bare wind turbine.

(**a**) (**b**) (**c**)

Figure 7. Configurations of Wind-Lens turbines: (**a**) long-type, (**b**) compact-type. See Table 2 for definitions of the symbols used in the figure.

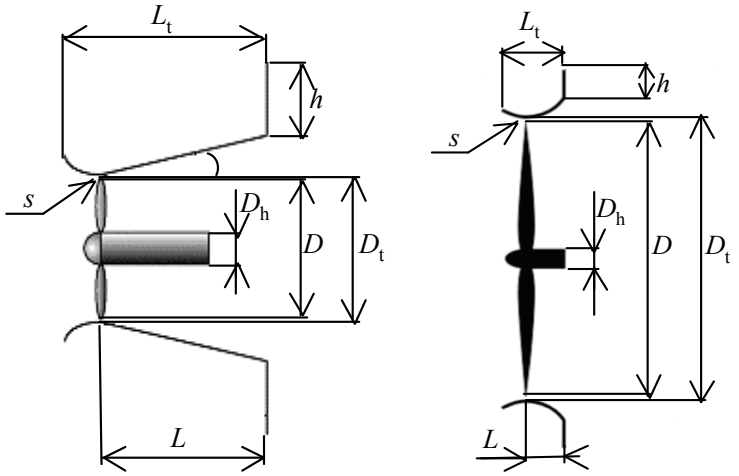

(**a**) (**b**)

3. Simulation Results for the Flow around the Blade Tip of a Long-Type Wind-Lens Turbine

A simulation of the flow around the blade tip of a long-type Wind-Lens turbine is conducted. Figure 8 shows the vortex structures from this simulation. The circumferential vortices are identified using the λ_2 identification method [13]. In Figure 8, the vortices are colored based on the circumferential direction of the vorticity. The vortices colored in blue are those which flow from the upstream side of the blade tip to the downstream side. These vortices are blade tip vortices since they come around from the upstream side of the blade to the downstream side of the blade. A strong counter-rotating vortex structure (red in Figure 8) is generated alongside the blade tip vortex between the blade tip and the inner surface of the diffuser. This counter-rotating vortex is probably induced by the interaction of the tip vortex and the inner surface of the diffuser. These vortex structures are qualitatively consistent with those observed in the wind tunnel experiment performed by Sato *et al.* [14] as seen in Figure 9. This experiment was reported by Abe *et al*. [15]. Figure 8 shows that, although the blade tip vortex and the induced vortex are in alignment at first, eventually the induced vortex is partially rolled up by the blade tip vortex. Further downstream, the blade tip vortex also rolls up and forms a helical structure with the induced vortex. The blade tip vortex and the induced vortex are mutually weakened in this process and dissipate before they reach the end of the diffuser.

Figure 8. Simulation results for the long-type Wind-Lens turbine: θ-component of the vorticity inside a long-type Wind-Lens turbine. *x*: inflow direction; *r*: radial direction; θ: circumferential direction.

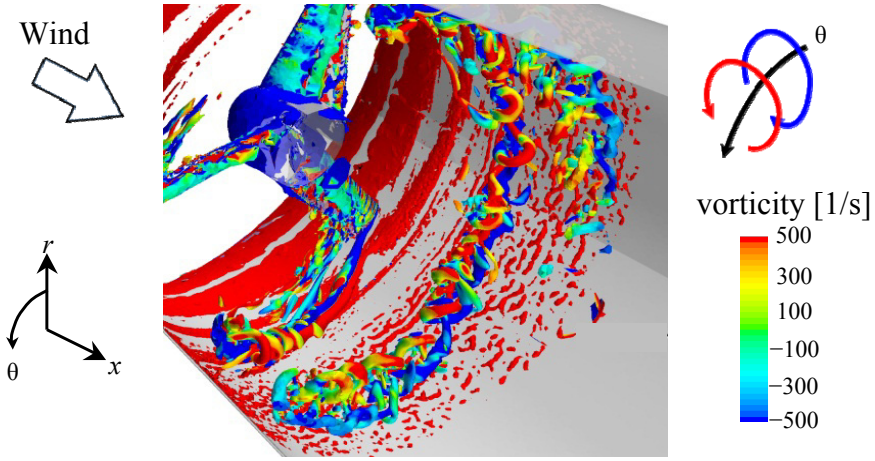

Figure 9. Wind tunnel experimental results for the long-type Wind-Lens turbine: θ-component of the vorticity inside a long-type Wind-Lens turbine [14].

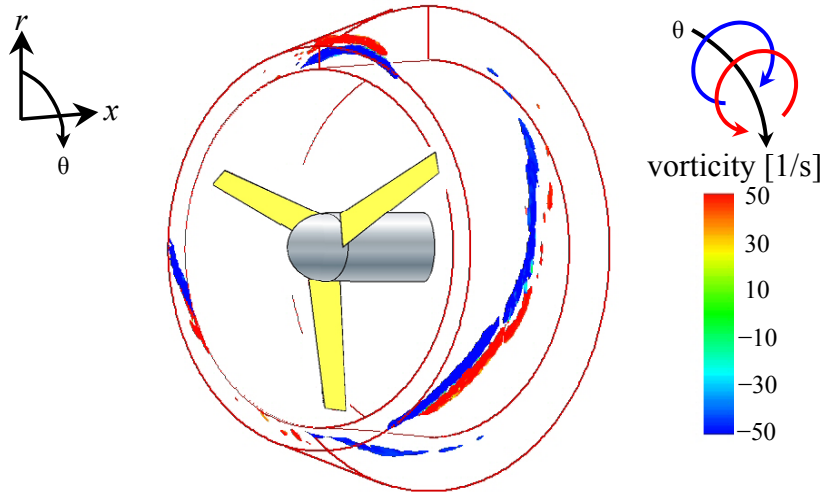

The behavior of these vortices is qualitatively consistent with results from wind tunnel experiments as shown in Figure 10a [14,16]. For comparison, Figure 10b shows the vortices observed in the same wind tunnel experiments for the bare wind turbine. In the wind tunnel experiments, the configuration of the bare turbine was the same as that of the long-type Wind-Lens turbine without the diffuser shroud. Furthermore, the Wind-Lens turbine used in the wind tunnel experiments was identical to that used in the present simulation. The arrows in Figure 10 represent the flow velocity. In the wind tunnel experiments, conditional sampling was used to identify the mean vorticity field while the blades were rotating. Similar to the numerical results, induced vortices with counter-vorticity appeared between the blade tips and the inner surface of the diffuser in the wind tunnel experiments, as seen in the middle panel of Figure 10a. Downstream, the tip vortices became very weak in the case with the brimmed-diffuser shroud (Figure 10a) in comparison to the tip vortices in the case without the shroud (Figure 10b), which is also qualitatively consistent with the results of the present study as will be described in Section 4.2.

Figure 10. (**a**) Wind tunnel experimental results for the long-type Wind-Lens turbine: *x*-component of the vorticity (colors) and velocity (vectors) in *r*-θ cross-sections; (**b**) Same as Figure 10a except for the bare wind turbine [14,16].

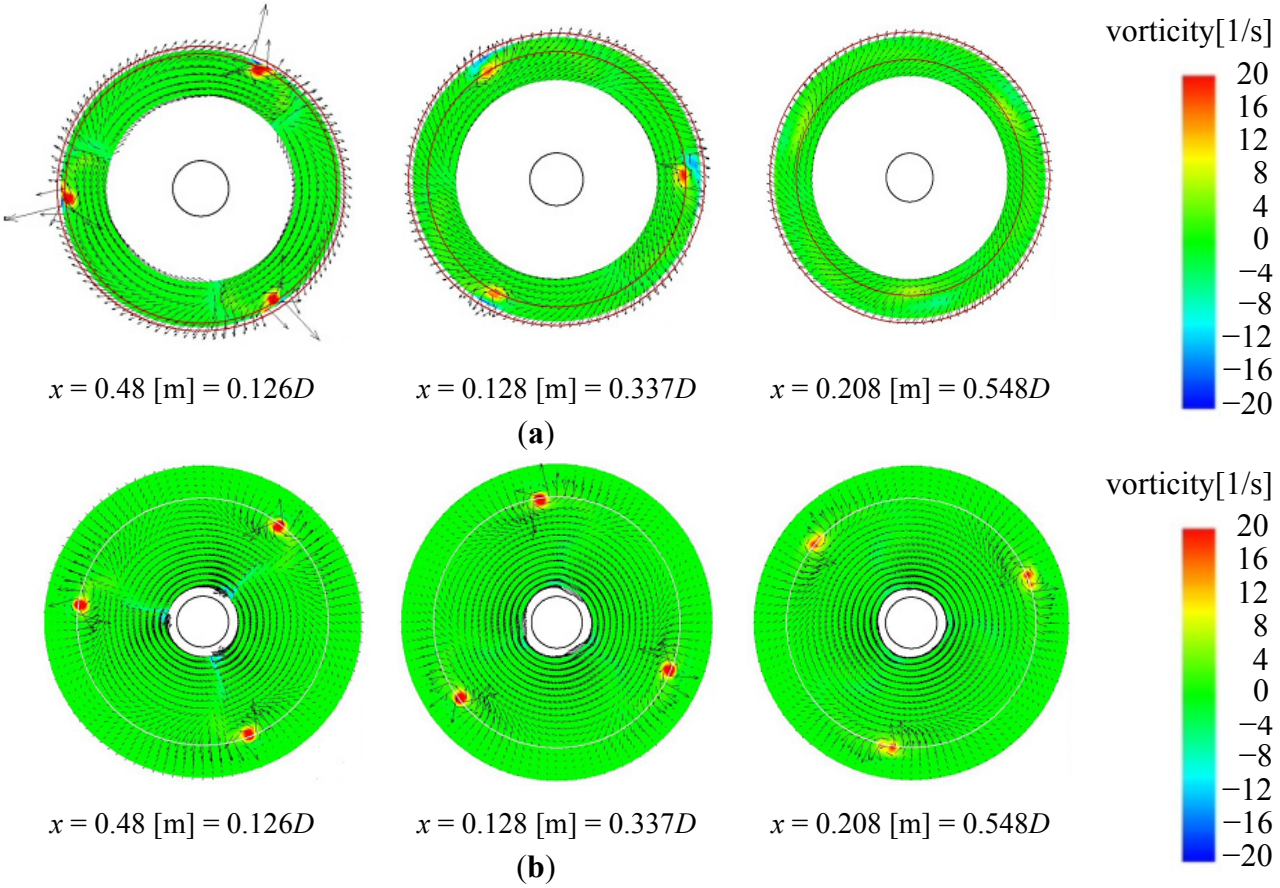

In addition, in case of the bare wind turbine, the shapes of the blade tip vortices in the middle panel of Figure 10b are almost same as that in the upstream side as seen in the left panel of Figure 10b. However, in case of the long-type Wind-Lens turbine, the shapes of the blade tip vortices in the middle panel of Figure 10a are different from that in the upstream side as seen in the left panel of Figure 10a. This result of the long-type Wind-Lens turbine suggests that the blade tip vortices are interfered with by the induced vortices.

Subsequently, the behavior of these vortex structures is examined in detail. Figure 11 shows a contour plot of the circumferential vorticity at θ = 10°, 20°, 30°, 40°, and 50° of separation from the blade's leading edge. The induced vortex (red) is likely generated by the blade tip vortex (blue) within the boundary layer of the inner surface of the diffuser, as shown for θ = 10°. From θ = 10° to 50°, *i.e.*, as the blade rotates away from a particular position on the inner surface of the diffuser, the boundary layer over that position becomes thinner. The thinning of the boundary layer likely occurs as a result of the generation of the induced vortex. This thinning of the boundary layer in turn suppresses flow separation from the inner surface of the diffuser. Because the flow separation is suppressed, the pressure recovery from the diffuser entrance to the exit improves, which contributes to the Wind-Lens turbine's ability to efficiently collect and accelerate the incoming flow. Although blade tip vortices are a source of noise and a cause of power loss for wind turbines, these vortices may contribute to the improvement of the collection and acceleration of the incoming flow observed in Wind-Lens turbines.

Figure 11. θ-component of the vorticity inside the long-type Wind-Lens turbine including that of the blade tip vortex and the counter-rotating vortex.

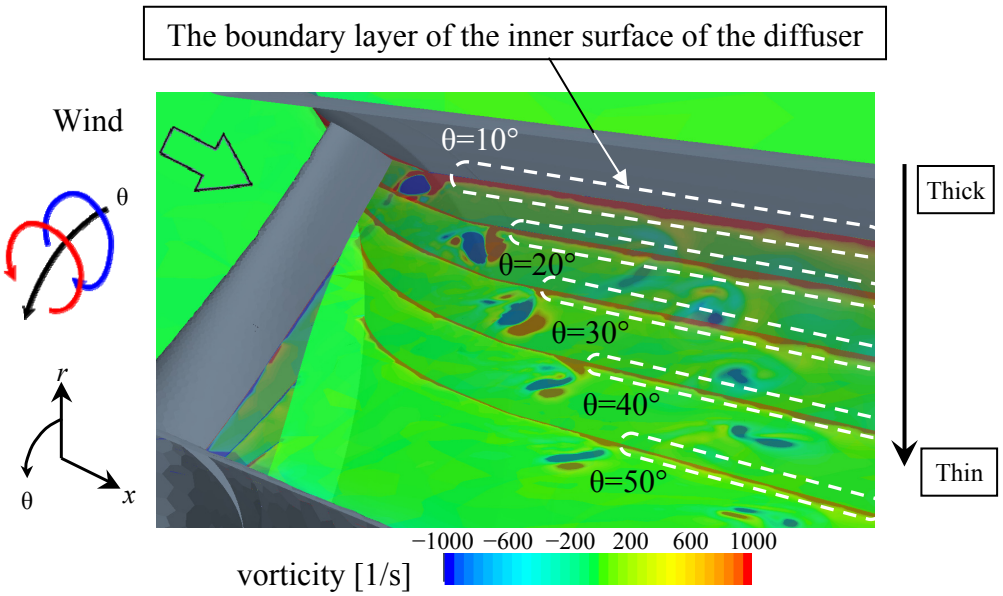

4. Simulation Results of the Flow around a Compact-Type Wind-Lens Turbine

4.1. Simulation Results of the Flow around the Blade Tip of a Compact-Type Wind-Lens Turbine

Similarly to the case with a long-style Wind-Lens turbine, a simulation of the flow around the blade tip of a compact-style Wind-Lens turbine is conducted. Figure 12 shows the vortex structures from this simulation. As with the long-type Wind-Lens turbine, the circumferential vortex is identified using the λ_2 identification method [13]. Blade tip vortices (blue) and the induced vortices (red) are also present in this case (Figure 12). Just as was the case with the long-type wind turbine, the blade tip vortex and the induced vortex are in alignment at first, and eventually the induced vortex is partially rolled up by the blade tip vortex.

Although the blade tip vortex and the induced vortex are mutually weakened in the above process, they do not dissipate before they reach the end of the diffuser because the diffuser length is shorter than that of the long-type diffuser and is shorter than the distance required for the vortices to dissipate. After the vortices flow out of the diffuser, they dissipate due to interference with the vortices separating from the inside of the diffuser.

Next, the behavior of the blade tip vortex is examined in detail. Figure 13 shows a contour plot of the circumferential vorticity at θ = 10°, 20°, 30°, and 40° of separation from the blade's leading edge. Similarly to the long-type Wind-Lens turbine, the induced vortex (red) is presumably generated by the blade tip vortex (blue) within the boundary layer of the inner surface of the diffuser. In addition, as the blade rotates away from a particular position on the inner surface of the diffuser, the boundary layer over that position becomes thinner.

Figure 12. θ-component of the vorticity inside a compact-type Wind-Lens turbine. *x*: inflow direction; *r*: radial direction; θ: circumferential direction.

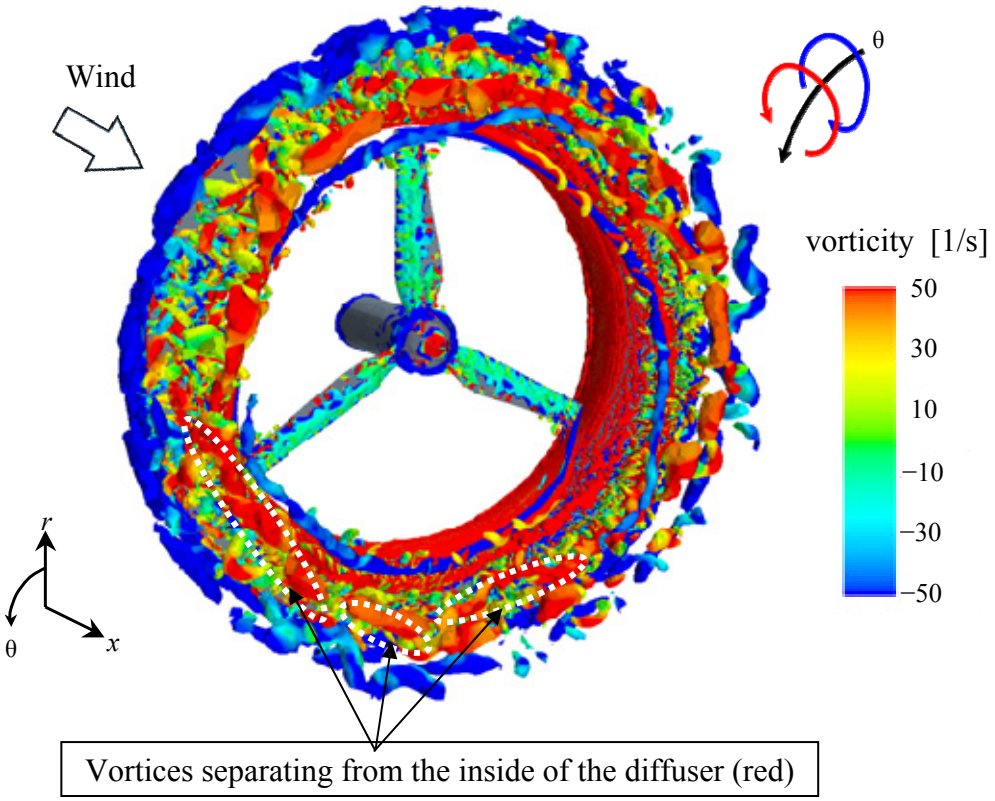

Figure 13. θ-component of the vorticity inside the compact-type Wind-Lens turbine including that of the blade tip vortex and the induced counter-rotating vortex.

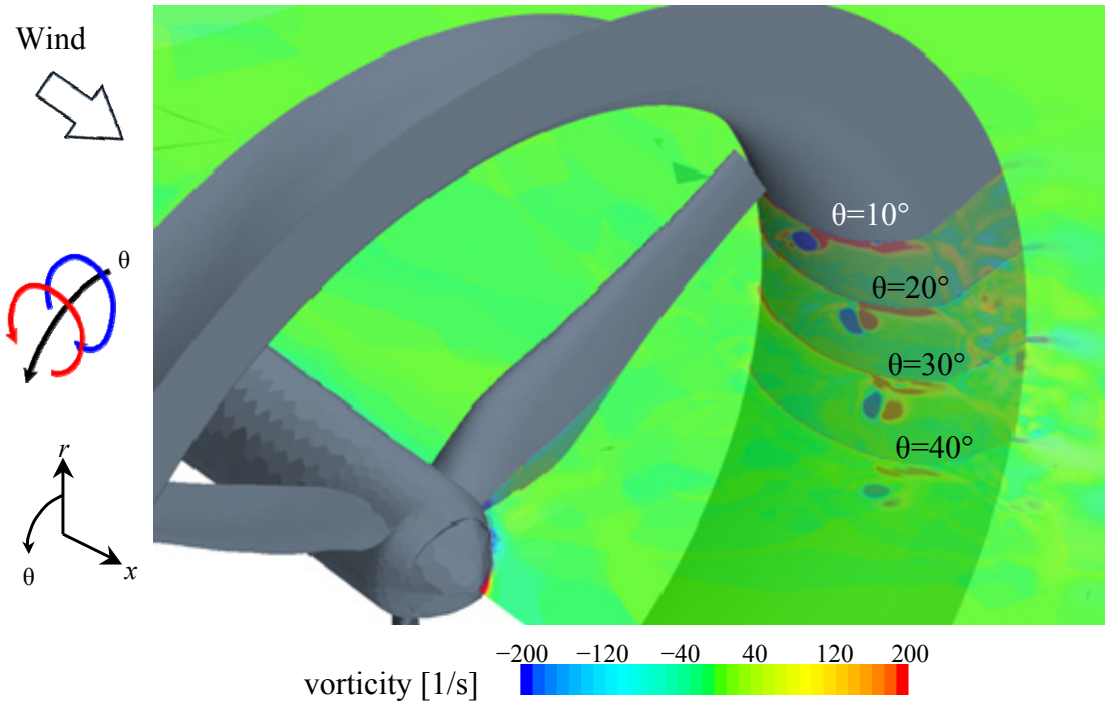

4.2. Comparison of the Flow around a Compact-Type Wind-Lens Turbine and the Flow around a Bare Wind Turbine

The blade tip vortex of a compact-type Wind-Lens turbine is compared with that of a bare wind turbine. Figure 14 shows contour plots of the x-component of the vorticity on an r-θ cross-section at x = 0.2 m (= 0.08D).

Figure 14. Comparison of the x-component of the vorticity in r-θ cross-sections between (**a**) the compact-type Wind-Lens turbine; and (**b**) the bare wind turbine at x = 0.2 m = 0.08D.

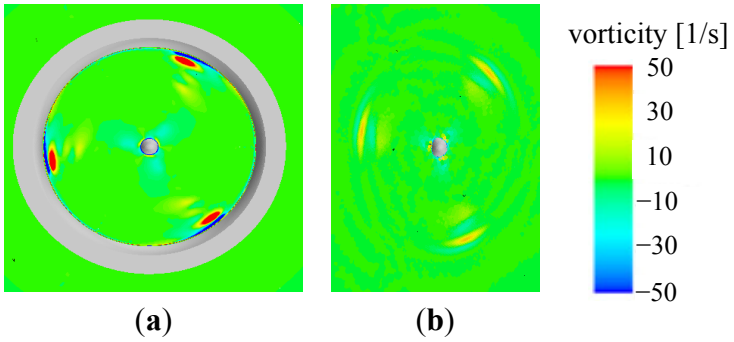

This figure shows that the Wind-Lens turbine generates stronger blade tip vortices (red) than the bare wind turbine. This is because the inflow, which is collected and accelerated by the Wind-Lens, is strengthened especially near the inside wall of the diffuser. This phenomenon can be seen in Figure 15, which depicts the wind velocity distribution at x = 0.0588D measured in a wind tunnel experiment [17]. Figure 14 also shows that, in the case of the Wind-Lens turbine, induced counter-rotating vortices (blue) appear between the blade tip and the inner surface of the diffuser.

Figure 15. Distribution of the x-component of the wind velocity, u, at x = 0.0588D for the compact-type Wind-Lens turbine as measured in a wind tunnel experiment [17].

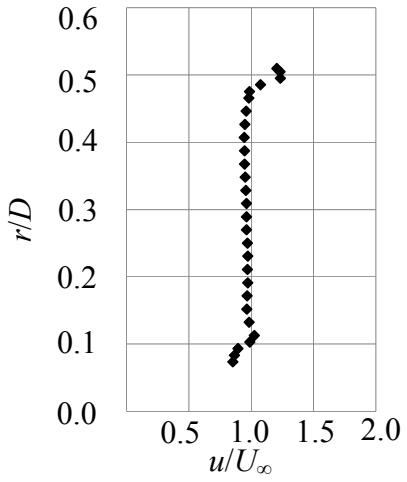

The Wind-Lens turbine generates strong blade tip vortices, however, the vorticity decreases by a larger amount over the same distance in the compact-type Wind-Lens turbine compared to the bare wind turbine (Figure 16). Additionally, the vortices in the Wind-Lens turbine are weaker than those in the bare wind turbine near x = 0.75 m and cannot be identified past approximately x = 0.75 m.

Conversely, the blade tip vortices of the bare wind turbine are identifiable at this downstream distance. The present numerical results show good agreement with the results from the wind tunnel experiment as described in Section 3.

Figure 16. Comparison of the θ-component of the vorticity between the compact-type Wind-Lens turbine and the bare wind turbine.

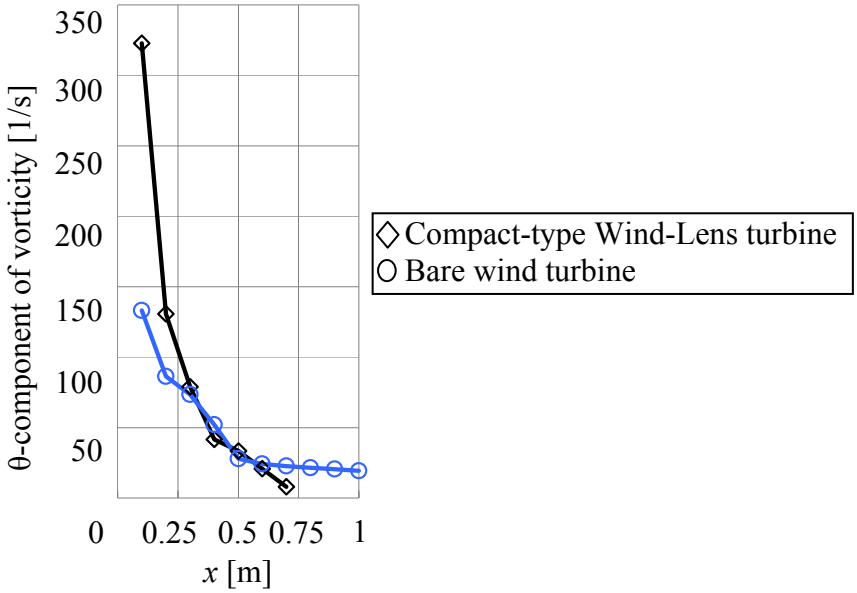

5. Conclusions

To clarify the behavior of the blade tip vortices of a wind turbine equipped with a brimmed-diffuser shroud, a "Wind-Lens turbine", we conducted a three-dimensional LES simulation using a moving boundary technique. We found that the blade tip vortices induce counter-rotating vortices between the blade tips and the inner surface of the diffuser and that the blade tip vortices are weakened by the interference with the induced vortices. First, the flows around the blade tips of a long-type and a compact-type Wind-Lens turbine are summarized below:

a. In addition to the blade tip vortex, an induced vortex rotating in the opposite direction appears alongside the blade tip vortex between the blade tip and the inner surface of the diffuser. These vortices are qualitatively consistent with those observed in a past wind tunnel experiment [14].
b. The induced vortex is presumably generated by the blade tip vortex within the boundary layer of the inner surface of the diffuser. As a result of the generation of the induced vortex, flow separation from the inner surface of the diffuser is suppressed, and collection and acceleration of the approaching wind is enhanced.
c. In the case of the long-type Wind-Lens turbine, the blade tip vortex and the induced vortex are mutually weakened and dissipate before they reach the end of the diffuser.
d. In the case of the compact-type Wind-Lens turbine, the induced vortex is partially rolled up by the blade tip vortex and these vortices are mutually weakened. However, neither of the vortices dissipate before they reach the end of the diffuser because the diffuser length is shorter than that of the long-type Wind-Lens turbine and is shorter than the distance required for the

vortices to dissipate. After the vortices flow out of the diffuser, they dissipate due to interference with the vortices separating from the inner surface of the diffuser.

Second, the differences between the flow around a compact-type Wind-Lens turbine and the flow around a bare wind turbine are summarized below:

a. The compact-type Wind-Lens turbine generates stronger blade tip vortices than the bare wind turbine because the inflow in the Wind-Lens turbine is accelerated especially near the inner surface of the shroud.
b. In the case of the compact-type Wind-Lens turbine, the strong blade tip vortices are greatly weakened by the interference with the induced vortex within a short distance. Conversely, the blade tip vortices of the bare wind turbine remain identifiable further downstream than those of the compact-type Wind-Lens turbine.

References

1. Gilbert, B.L.; Foreman, K.M. Experiments with a diffuser-augmented model wind turbine. *Trans. ASME J. Energy Resour. Technol.* **1983**, *105*, 46–53.
2. Ohya, Y.; Karasudani, T.; Sakurai, A.; Abe, K.; Inoue, M. Development of a shrouded wind turbine with a flanged diffuser. *J. Wind Eng. Ind. Aerodyn.* **2008**, *96*, 524–539.
3. Ohya, Y.; Karasudani, T. A shrouded wind turbine generating high output power with wind-lens technology. *Energies* **2010**, *3*, 634–649.
4. Fukuoka City's Home Page [in Japanese]. Available online: http://www.city.fukuoka.lg.jp/data/open/cnt/3/31055/1/H23hakatawanPJacess3_5.pdf (accessed on 26th May 2012).
5. Morris, P.J.; Long, L.N.; Brentner, K.S. An aeroacoustic analysis of wind turbine. In *Proceedings of 42nd AIAA Aerospace Sciences Meeting and Exhibit*, Reno, NV, USA, 5–8 January 2004.
6. Brooks, T.F.; Marcolini, M.A. Airfoil Tip vortex formation noise. *AIAA J.* **1986**, *24*, 246–252.
7. Arakawa, C.; Fleig, O.; Iida, M.; Shimooka, M. Numerical approach for noise reduction of wind turbine blade tip with earth simulator. *Earth Simulat.* **2005**, *2*, 11–33.
8. Abe, K.; Ohya, Y. An investigation of flow fields around flanged diffusers using CFD. *J. Wind Eng. Ind. Aerodyn.* **2004**, *92*, 315–330.
9. Abe, K.; Nishida, M.; Sakurai, A.; Ohya, Y.; Kihara, H.; Wada, E.; Sato, K. Experimental and numerical investigations of flow fields behind a small wind turbine with a flanged diffuser. *J. Wind Eng. Ind. Aerodyn.* **2005**, *93*, 951–970.
10. Ohya, Y.; Uchida, T.; Karasudani, T.; Hasegawa, M.; Kume, H. Numerical studies of flow around a wind turbine equipped with a flanged-diffuser shroud using an actuator-disk model. *Wind Eng.* **2012**, *36*, 455–472.
11. Troldborg, N.; Sorensen, J.N.; Mikkelsen, R. Actuator line simulation of wake of wind turbine operating in turbulent inflow. *J. Phys. Conf. Ser.* **2007**, *75*, 012063:1–012063:15.
12. Nicoud, F.; Ducros, F. Subgrid-scale stress modeling based on the square of the velocity gradient tensor Flow. *Turbul. Combust.* **1999**, *62*, 183–200.
13. Jeong, J.; Hussain, F. On the identification of a vortex. *J. Fluid Mech.* **1995**, *285*, 69–94.

14. Sato, K.; Abe, K. An Experimental Study of Blade tip Vortex of a Wind Turbine with a Flanged Diffuser [in Japanese]. Master's Thesis, Kyushu University, Fukuoka, Japan, 2005.
15. Abe, K.; Kihara, H.; Sakurai, A.; Nishida, M.; Ohya, Y.; Wada, E.; Sato, K. An experimental study of tip-vortex structures behind a small wind turbine with a flanged diffuser. *Wind Struct.* **2006**, *9*, 413–417.
16. Wada, E.; Nishida, M.; Abe, K. An Experimental Study of Flow around a Wind Turbine with a Flanged Diffuser [in Japanese]. Master's Thesis, Kyushu University, Fukuoka, Japan, 2004.
17. Hasegawa, M.; Ohya, Y.; Karasudani, T. Research on the optimal element design of a wind-lens turbine and application of Wind-Lens to a large-scale wind turbine [in Japanese]. Master's Thesis, Kyushu University, Fukuoka, Japan, 2006.